ELSEVIER

Journal of Nuclear Materials 318 (2003) 167–175

journal of nuclear materials

www.elsevier.com/locate/jnucmat

Neutronics calculation, dosimetry analysis and gas measurements of the first SINQ target irradiation experiment, STIP-I

Y. Dai [a,*], Y. Foucher [a,b], M.R. James [c], B.M. Oliver [d]

[a] *Paul Scherrer Institut, CH-5232 Villigen PSI, Switzerland*
[b] *Subatech, EMN, 4 rue Alfred Kastler, P.O. Box 20722, 44307 Nantes cedex, France*
[c] *Los Alamos National Laboratory, Los Alamos, NM 87545, USA*
[d] *Pacific Northwest National Laboratory, Richland, WA 99352, USA*

Abstract

To precisely determine the damage, helium and hydrogen production in the specimens irradiated in Swiss Spallation Neutron Source Target-3, calculations with the MCNPX code, dosimetry analysis and helium/hydrogen measurements have been performed. The MCNPX calculations agree well with the former calculations performed with the LAHET code. The preliminary analysis of dosimetry foils demonstrates that the unfolded proton and neutron spectra at limited positions are close to calculated values. In general the measured He concentrations were consistent with the calculated values. Some discrepancy between the measured and calculated values is believed due to the actual proton beam geometry being different from that used for the calculation. The hydrogen concentration measured in samples irradiated at $<\sim$100 °C is close to the calculated. The differences between the measured and calculated values for samples irradiated at higher temperatures can be attributed largely to the effects of hydrogen diffusion. The results indicate that at $>\sim$250 °C, only a small amount of hydrogen remains in the samples.

1. Introduction

To establish a necessary materials database for the application of spallation neutron sources and other accelerator driven systems, two irradiation experiments have been performed in different targets in the Swiss Spallation Neutron Source (SINQ) at the Paul Scherrer Institut. The first irradiation (STIP-I) was done in SINQ Target-3, which was made of Zircaloy-2 rods, between 1998 and 1999 [1].

For this irradiation, the proton and neutron flux distributions at different positions in the target were initially calculated with the LAHET code [1,2]. To confirm and also upgrade that calculation, new calculations have been performed using the MCNPX code. In addition, about 80 dosimetry discs irradiated with the specimens in the target have been counted. The corresponding data were analyzed with the STAYSL2 code from LANL [3]. The data from the unfolded spectra have been compared with the calculations. Since the He and H contents of samples can be precisely determined using mass spectrometry methods [4,5], 12 irradiated samples of different materials from different positions in the target were also analyzed. The measurements provide not only data for comparison with calculated gas contents, but also valuable information about hydrogen retention in materials at elevated temperatures in spallation sources.

2. Target and incident proton beam

The SINQ target is oriented vertically, as illustrated schematically in Fig. 1. The proton beam is injected

* Corresponding author. Tel.: +41-56 310 4171; fax: +41-56 310 2485.
E-mail address: yong.dai@psi.ch (Y. Dai).

0022-3115/03/$ - see front matter © 2003 Elsevier Science B.V. All rights reserved.
doi:10.1016/S0022-3115(03)00099-0

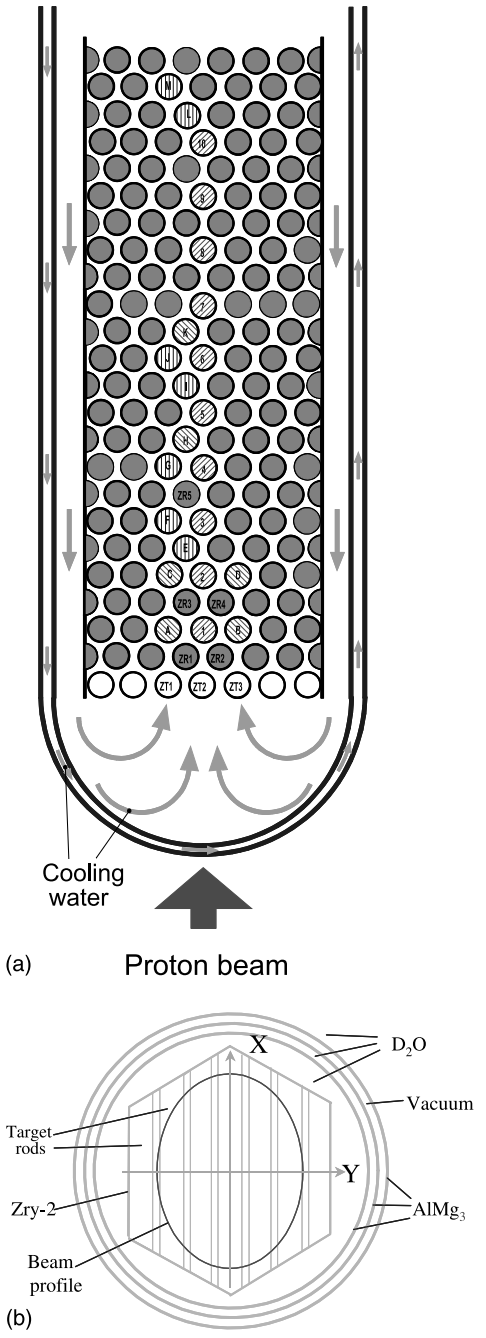

Fig. 1. (a) Sketch showing the positions of specimen rods in the lower part of the target. Note that there are actually 9 or 10 rods in one row. (b) Sketch showing the proton beam distribution at the cross-section of the target.

from the bottom into the target. The lower part of the target consists of an inner target module and an outer safety container. For Target-3, the target module was comprised of several hundred Zircaloy-2 rods (filled circle), 23 specimen rods (filled circles with numbers 1–10 and A–M) and several Zircaloy-2 tubes (empty circles). The safety container is a double-walled structure fabricated of $AlMg_3$ alloy. Both the module and safety container were cooled by heavy water (D_2O) during operation, as illustrated in the figure.

The horizontal cross-section of the target module is hexagonal in shape, as shown in Fig. 1(b). The intensity and profile of the incident proton beam depends on the thickness of Target-E which is a graphite target, 6 or 4 cm thick, installed in the beam line in front of the SINQ target. The beam profile can be represented as a truncated 2-dimensional Gaussian distribution:

$$I = \frac{I_0}{2\pi\sigma_x\sigma_y}\exp\left(-\frac{x^2}{2\sigma_x^2}\right)\exp\left(-\frac{y^2}{2\sigma_y^2}\right)\exp\left(1-\frac{c^2}{2}\right), \quad (1)$$

where $c = 2$, $I_0 \approx 0.85$ mA, $\sigma_x = 3.56$ cm and $\sigma_y = 2.12$ cm for the 6 cm Target-E case, and $I_0 \approx 1.04$ mA, $\sigma_x = 3.31$ cm and $\sigma_y = 1.9$ cm for the 4 cm Target-E case. During the actual beam time of about 14 months, the 6 cm Target-E was used for the first 12 months and the 4 cm Target-E was used for the last 2 months [1].

3. Proton and neutron spectra of specimen rods

In general, the proton and neutron spectra calculated with the MCNPX code agree well with those obtained from the LAHET calculation. For simplicity, only those results calculated for the 6 cm Target-E case are discussed in this section. Fig. 2 presents the differential proton flux at the central positions of rods 1, 5 and 10. The spectra calculated with MCNPX resemble those from LAHET. However, the energy windows of the

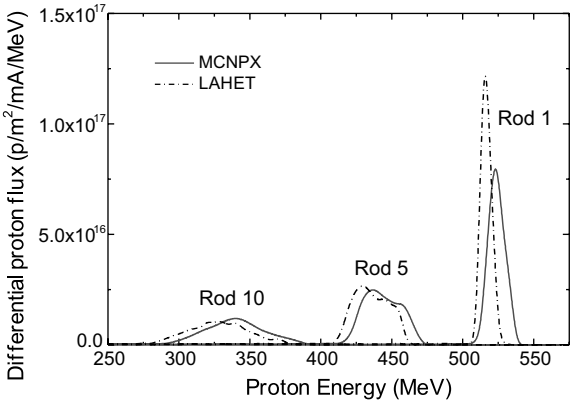

Fig. 2. A comparison of proton spectra calculated with the MCNPX and LAHET codes for the central positions of rods 1, 5 and 10.

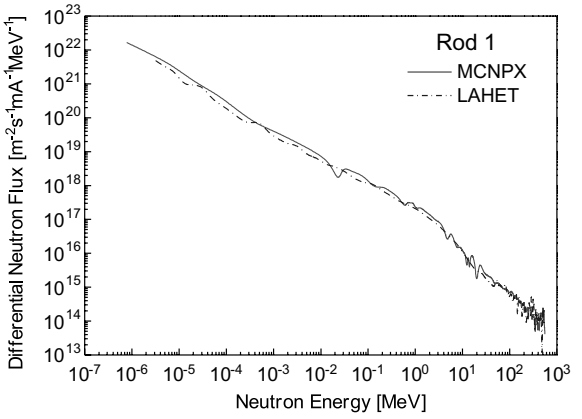

Fig. 3. A comparison of proton spectra calculated with the MCNPX and LAHET codes for the central positions of rod 1.

peaks of all the rods have the same shift of about 5–10 MeV to higher energy values. This may be due to the different incident proton energies used in the two calculations, 570 MeV for LAHET case and 575 MeV for MCNPX case. Fig. 3 shows the differential neutron spectra at the center of rod 1 calculated with both codes. It can be seen that both spectra agree quite well. The integrated fluxes of proton, (total) neutron and fast neutron at the central positions of rods 1, 5 and 10 are plotted in Fig. 4. As can be seen, the differences between the values calculated with the different codes are very small, i.e., <5%.

The shapes of the proton and neutron spectra at different positions along a rod are essentially the same as at the center. The flux decreases with increasing distance from the center. In addition, in the 4 cm Target-E case the shapes of the spectra at different positions in the target are similar to those in the 6 cm Target-E, except for a slight difference in the height of the peaks, which is due to the different geometries of the incident proton beam.

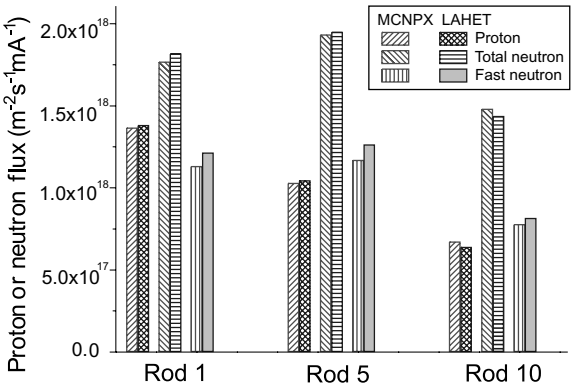

Fig. 4. A comparison of fluxes of protons, (total) neutrons and fast neutrons calculated with the MCNPX and LAHET codes for the central positions of rods 1, 5 and 10.

4. Total proton and neutron fluences, displacement, helium and hydrogen production

As mentioned above, the irradiation was composed of two parts differentiated by the proton beam current and geometry as a result of the change of Target-E. Therefore, the total proton and neutron fluences were calculated from the two beam conditions based on the total proton charge received for each beam condition. The final results are given in Fig. 5, which shows the proton and fast ($E > 0.1$ MeV) neutron fluences for the 10 specimen rods at different positions along the rods.

The cross-sections for various materials were computed previously as part of the APT program to evaluate radiation damage in various materials [6]. These calculations were originally performed with MCNPX version 2.1.5 and did not include the more recent LA150 evaluated libraries. As such, these cross-sections for H, He and dpa relied on evaluated libraries below 20 MeV and physics models above 20 MeV. They were calculated using a material mixture of the alloy desired (e.g. SS 316)

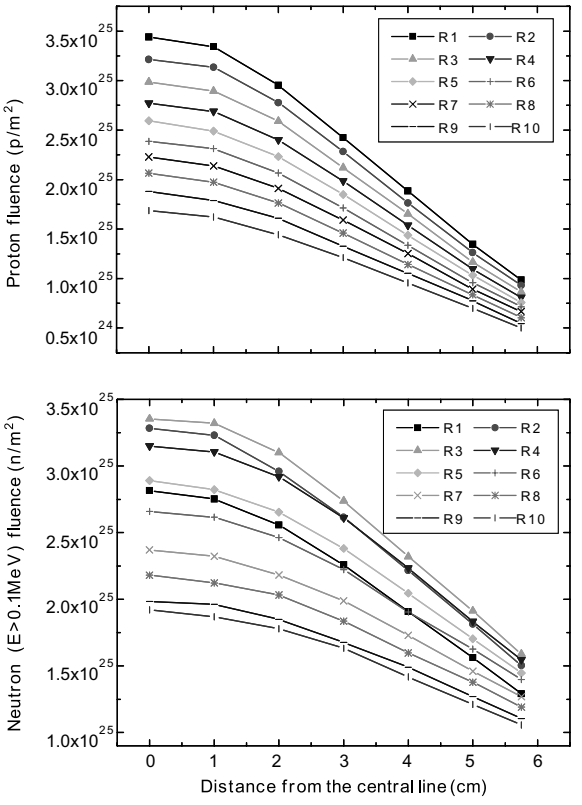

Fig. 5. Calculated proton and neutron fluence distributions along the axial position of each specimen rod.

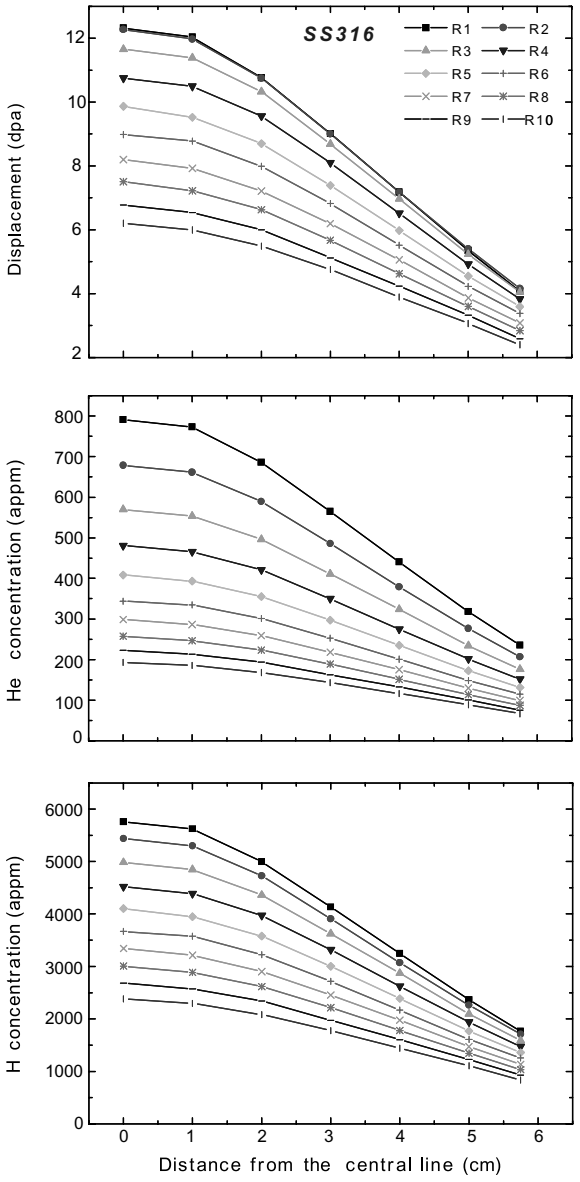

Fig. 6. Calculated dpa, He and H distributions along the axial position of each specimen rod for SS 316L.

and a source of mono-energetic neutrons or protons impinging on a small volume of material. The final cross-sections were derived from a tally of the damage energy and gas production in the sample volume. Runs of different source particle energies were used to construct the energy dependence of the cross-sections desired. The He and H cross-section data have been upgraded based on the measurement results from the APT irradiation program [7]. The cross-sections for materials Al 6061, SS 316L, 9Cr–1Mo, F82H, Inconel 718 and Zircaloy-4 were used in this work. As an example, Fig. 6 illustrates the distributions of dpa, He and H production in the specimen rods for SS 316L.

The spatial distribution of dpa, He and H data for each rod can be fit with Gaussian functions. From these Gaussian fittings the dpa, He and H for each specimen location can be easily calculated.

5. Dosimetry analysis

In order to analyze the proton and neutron spectra, approximately 100 activation discs of pure Al, Au, Cu, Co, Fe, Nb, Ni, and Ti were placed at the center and edge positions of rods 1, 3, 4 and 10 or in some cases along the rods (see Fig. 7). Unfortunately, due to an unintended over-focused beam excursion, the activation discs at the center position of rods 1 and 3 were completed lost. In all, about 85 discs were available for analysis, but only about 60 discs could be clearly identified. The reason for this was the presence of copper oxide which inhibited identification of some Cu foils, and the activity of Co foils was too high for safe handling. These issues greatly reduced the number of useful foils and nuclear interactions that could be used. It turned out that only a few locations could be completely analyzed to refine the knowledge of fluxes in those locations. These locations were the edge locations in rods 1, 2, 3, the center location in tube 4 and the center and edge locations of rod 10.

The dosimetry analyses used the STAYSL2 code [3] developed at Los Alamos for analysis of the LANSCE/APT irradiations. Additional cross-sections for $Ti \rightarrow Na\text{-}22$, $Ti \rightarrow Sc\text{-}46$, $Fe \rightarrow Sc\text{-}46$, and $Au \rightarrow Ag\text{-}110m$ were also added. Other reactions were tried but proved to be unreliable or inconsistent with the data. These included: $Cu \rightarrow Sc\text{-}46$, $Ni \rightarrow Mn\text{-}54$, $Nb \rightarrow Nb\text{-}94$, $Au \rightarrow Au\text{-}195$. The results show that:

(1) At the edge position of rod 1, the proton fluence is somewhat lower (~30%) than calculations, with higher neutron flux across all energies by a factor of 1.5–2.0.
(2) At the edge of rod 2, the proton flux is also lower by a small factor (~10–15%) as compared to the calculations. Neutron fluxes also appear to be higher in the 1–40 MeV range, by about 50%. Higher energy (40–500 MeV) neutron fluxes are lower than calculated.
(3) At the edge of rod 3, the results suggest a lower proton energy and slightly lower fluence than the calculations. Neutron fluxes showed a general increase at energies of 1–50 MeV, up to a factor of 2. All other energies showed little change.
(4) At the center of rod 4, the results suggest a lower proton energy (440 → 420 MeV) and a slightly lower fluence. The neutrons were also higher in total flux

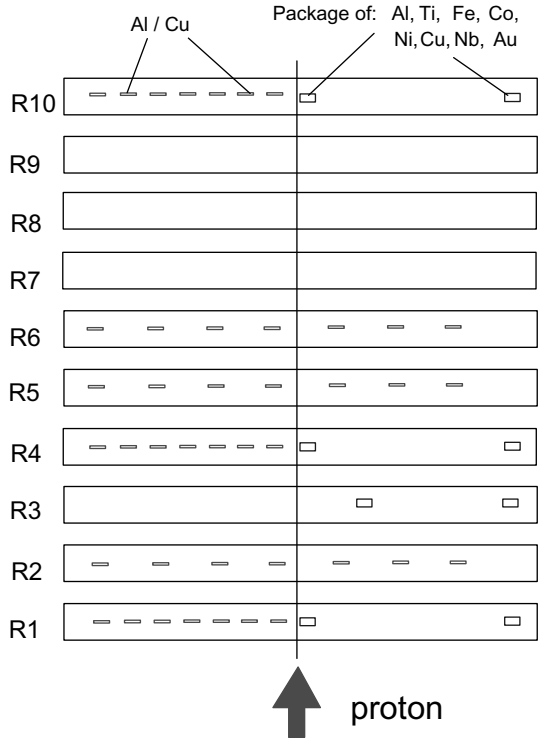

Fig. 7. A sketch showing the positions of activation discs in SINQ Target-3.

at higher energies (>200 MeV), although they are difficult to separate from the protons in this region. No information on the low energy neutrons was available.

(5) At the center of rod 10, the original calculated spectra and the unfolded spectra are given in Figs. 8 and 9 for neutrons and protons respectively. In Fig. 8, the unfolded proton spectrum is similar to the calculated. The flux estimates are about the same as the calculated from MCNPX. As shown in Fig. 9, unfolded neutron fluxes are approximately the same as the calculated fluxes at low energies, but above about 10 MeV, they are lower than the calculated values by approximately 50%. The increase in the thermal flux region is inferred from the increased relative burn-up of Na-22 in the Al foils.

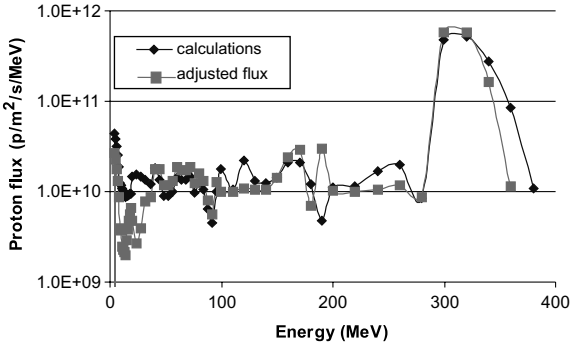

Fig. 8. Comparison of the proton fluxes unfolded from the activation results and calculated with MCNPX for the central position of rod 10. The uncertainties for the unfolded spectra should be considered to be 20–30%.

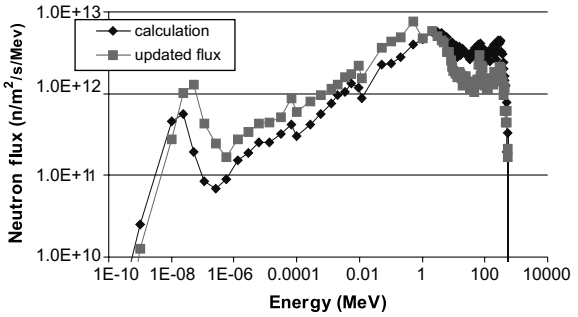

Fig. 9. Comparison of the neutron fluxes unfolded from the activation results and calculated with MCNPX for the central position of rod 10. The uncertainties for the unfolded spectra should be considered to be 20–30%.

(6) At the edge of rod 10, activation results suggest an increase in the proton energy from 300 to 320 MeV. The proton flux is lower than the calculated value by a factor of almost 25%. The neutron flux is higher by a factor of 2 at the lower energies (<40 MeV), but in good agreement between 40 and 200 MeV. At higher energies, the neutron flux is adjusted upwards.

The use of the Na-22 burn-up (the substantial decrease from the expected Na-22 activity) was the only information available for the thermal flux region. As mentioned, the activities of Co foils were far too high to handle and measure. Additionally, it was necessary to wait several months before the foils could be extracted from the target tubes, making some useful reactions like the Au → Au-198 reaction unusable due to decay. The Co-58 isotopes also experienced some burn-up, although the magnitude was much smaller than in the Na-22 case. No significant information about the thermal flux region could be derived.

The statistical uncertainties associated with the calculation of the flux using activation foils are combination of the uncertainties from the cross-sections, the flux calculations and the foils measurements. Although these are produced from STAYSL2 as nominal statistical errors for each flux energy bin, these numbers to not properly capture the true uncertainties from all sources. Systematic errors in the flux calculations are not captured, indeed this is part of what the foil analysis is trying to check. In addition, the flux energy bins

outnumber the number of foil reactions making the solution an underdetermined one. This is complicated by the dependent relationship of the flux in various energy groups to one another. The shape as well as the magnitude of the fluxes can effect adjacent or distant energy bins. Overall, the uncertainty associated with the unfolding process performed in this work can be estimated to be 20–30%; typical for other neutron spectra unfolding problems.

6. He and H measurements

He and H concentrations can be precisely determined using hot-vacuum extraction in combination with gas mass spectrometry. The details of the measurement techniques are described in [4,5]. In order to determine the He and H production at different positions in the target, seven F82H, two SS 316L, two Al and one $AlMg_3$ discs were analyzed at Pacific Northwest National Laboratory (PNNL). The 7 discs of F82H steel were selected from the center and edge areas of rods 1, 4, 5 and 10. Detailed information on the discs is given in Table 1.

Helium and hydrogen concentrations were measured in duplicate specimens from each of the 12 samples. Most of the samples were in the form of TEM-sized disks that had already been used for shear punch testing. The duplicate specimens were cut using small diagonal wire cutters from the remaining TEM material. Since the samples had been sandwiched during irradiation, no etching was done on the samples prior to segmentation. Prior to analysis, each specimen was rinsed in acetone and air-dried. The mass of each specimen was then determined using a calibrated microbalance. Mass uncertainty is estimated to be ±0.002 mg.

Mean helium concentration values for each of the 12 samples are given in Table 1, and ranged from 134 to 1047 appm. Helium isotopic ratios ($^4He/^3He$) for the samples ranged from ~10 to ~24, which is consistent with values observed for other high-energy proton-irradiated materials [7]. Reproducibility between the duplicate helium analyses averaged ~1%. The normal analysis system reproducibility for samples with known homogeneous helium content is ~0.5%, indicating very low flux gradients across the samples.

Hydrogen concentrations measured in the 12 samples are also given in Table 1. Mean hydrogen concentrations in the samples ranged from ~250 to ~1900 appm. Except for one sample, $AlMg_3$, reproducibility between the duplicate hydrogen analyses averaged ~24%, which is within the range of variability observed in measurements of a low-level standard hydrogen-containing steel at PNNL. The $AlMg_3$ sample showed a large variability in the initial set of duplicate analyses. This sample was analyzed a second time in duplicate and showed the same variability. Therefore, we have assumed that the two high values were the result of some surface contamination, although the nature and source of this contamination is not known.

7. Discussion and conclusions

7.1. Damage, helium and hydrogen calculations

The damage, He and H production was calculated largely using the cross-section data calculated directly

Table 1
He and H measurements on F82H, EN316LN and aluminum samples irradiated in SINQ Target-3

Sample	Material	Position rod/X (mm)	Irradiated temperature[a] (°C)	He (cal.) (appm)	He[b] (meas.) (appm) ±1%	H (cal.) (appm)	H (meas.) (appm) ±24%
P^{13}	F82H	R1/7.5	360	920	1117	4960	360
P^{20}	F82H	R1/57	110	275	226	1490	520
P^{1}	F82H	R4/15.5	295	580	669	3500	390
P^{17}	F82H	R5/4	140	550	706	3430	1100
P^{3}	F82H	R5/48.5	67	235	233	1500	1650
P^{15}	F82H	R10/11.5	200	225	377	1870	690
P^{b}	F82H	R10/55	90	82	147	750	730
J^{2}	EN316LN	R10/55	67	68	139	850	390
J^{6}	EN316LN	R4/19.5	280	420	707	3980	320
A^{18}	Al	R6/0	195	520	674	1310	1300
Al^{21}	Al	R5/55	75	165	187	425	775
$AlMg_3$	Al + 2.5%-Mg	Beam window	55	770	1125	2700	1900

[a] The values of the irradiation temperature in the table are the average values of the irradiation temperatures during the two irradiation periods. The difference of the irradiation temperatures in the two periods is about 15% of the average values [1].

[b] The sum of ^3He and ^4He.

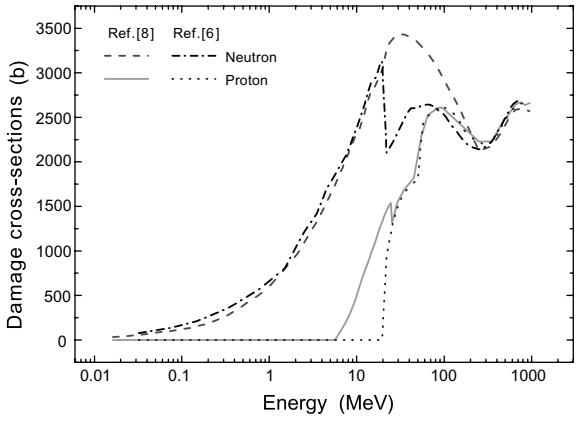

Fig. 10. Neutron and proton damage cross-sections for SS316 from [6,8].

from the MCNPX code. In previous work [1], for example, the damage for SS316 was calculated using the cross-section data from Wechsler [8], which was a combination of the results from SPECTER [9], LAHET and LA150 [10]. The main difference to the present work is that Wechsler's neutron damage cross-sections are higher in the energy range from 20 to about 200 MeV due to the results from LA150 and polynomial fitting, as shown in Fig. 10. Another difference occurs for proton damage cross-sections below 20 MeV. Due to facts that more than 90% of the neutron damage is contributed by those neutrons with energy below 20 MeV, and the energy of protons is above 300 MeV (Fig. 2), the difference in the dpa calculated using the two sets of cross-sections is negligible.

Like those shown in Fig. 10, there are large jumps in damage, He and H cross-sections at 20 MeV, which stem from difference in the SPECTRA data and LAHET data. Although the LA150 results improve the transition between the SPECTRA and LAHET data, the differences still remain (often the transition is shifted to 150 MeV). Nonetheless, as the energy range of the protons is largely above 300 MeV, and most of the neutrons are below 20 MeV, the data from SPECTRA and LAHET are satisfactory for the present calculations.

7.2. Dosimetry

Overall, the activation foils give exposed fluences which are very close to the calculated values. The experimental arrangement in the SINQ target is very favorable for the calculations as the rods and target have good alignment with the proton beam, there is very little y-axis variation in the sample distributions, and the target is thick relative to the particle ranges. Aside from small adjustments in the proton energy and fluence, and increases in the low-energy neutron flux, the overall agreements were very good in all cases.

The addition of Ti and Au foils provided additional reactions over the set of materials used in previous dosimetry at LANSCE [3], but ultimately little use was made of these data. The number of useful reactions for these two materials was limited, and the ones that were used did not reliably track with other reactions. More work is needed, particularly in the cross-section values, to get useful and reliable data from Ti and Au in the SINQ environment.

7.3. Helium and hydrogen measurements

In general the measured He concentrations were consistent with the calculated values. However, the differences are still significant. Fig. 11(a) shows the difference $(C_{\text{meas}} - C_{\text{cal}})/C_{\text{cal}}$ (where C_{meas} and C_{cal} are measured and calculated concentrations) at different positions in the target. Relative to the calculations, the data clearly indicate higher measured helium concentrations at the center of rod 1, and lower concentrations at the edge. The results from rod 5 are similar, only the difference becomes smaller at the edge position. In the case of rod 10, the situation is quite different. Here, the measured values at both center and edge are about 65% higher than calculated. This in spite of the fact that these cross-sections we updated based on measurements of the APT program [7]. However, the APT data was over the 600–800 MeV range for proton interactions, while here the energy for the protons in this case is 300–600 MeV. Other potential differences include the different microstructural trapping effects and further uncertainties in the flux calculations that could explain the differences in measured/calculated He content.

For rods 1 and 5, the higher He measured values at the center and the lower values at the edge may be due to inaccuracies in the incident proton beam geometry used for the calculation. The γ-scan of the Zircaloy-2 tube in the central column and first row gave $\sigma_x = 2.98$ cm, rather than 3.56 or 3.33 cm. This indicates that the actual beam size was much smaller than expected. In this case, it would be expected that the measured values would be higher at the center and lower at the edge. In addition, as was mentioned above, the dosimetry results also indicated that the proton fluence was somewhat lower ($\sim$30%) than calculations at the edge position of rod 1.

However, it is unclear why the differences increases with the depth into the target and why the differences at the edge positions increase faster than that at center positions. Nonetheless, it suggests that the calculations of neutron and proton spectra, and the cross-section data, both need to be improved.

Because of the differences between the measured and calculated helium concentrations, it is necessary to

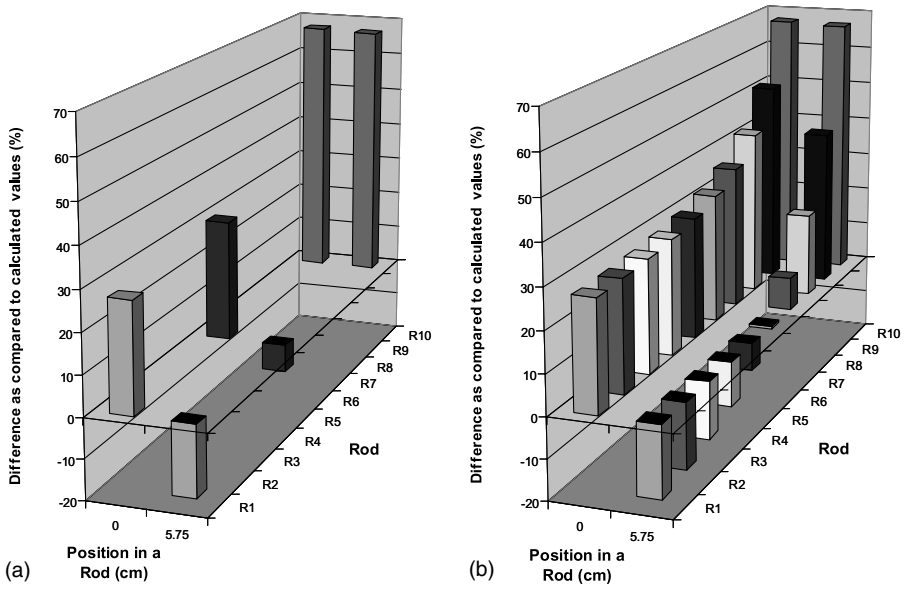

Fig. 11. The ratio of the measured He concentrations and the calculated He concentrations at different positions in the target. At the left (a) is the experimental data and at the right (b) is the fitted data using empirically determined functions (see text).

re-normalize the calculations based on the measured data. The data points for center or edge positions given in Fig. 11(a) can be fit with exponential functions verse the depth (or the rod number), as illustrated in Fig. 11(b) for all the 10 specimen rods. On the other hand, the differences along the same rod can be fit with a linear function. These fitting functions will be used to adjust the calculations for all positions in the present target. In principle the dpa data should be adjusted in the same way. This means that the dpa numbers of the samples in the central parts can be 20% higher than those shown in Fig. 6. However, it is not clear whether it is correct to do so since no reliable spectral data in the central positions of the first few rods (e.g. rod 1–4) were obtained from the dosimetry analysis. Therefore, in all work related to STIP-I (e.g. [11–13]) the dpa numbers are as calculated without any additional adjustment.

For the hydrogen concentration, the differences between the measured and calculated values can be attributed largely to the effects of irradiation temperature. In Fig. 12, the ratio of the measured-to-calculated values are plotted as a function of irradiation temperature. The general trend is clear: the hydrogen concentration decreases rapidly when the irradiation temperature increases. Particularly at temperatures above 250 °C, the measured hydrogen in the irradiated samples is around 300–400 appm (samples P^{13}, P^{1} and J^{2} in Table 1), which is not much higher than that typically seen in unirradiated material, about 140 appm [14]. This means that most of the irradiation-generated hydrogen diffuses out of the steel at these temperatures. This suggests that

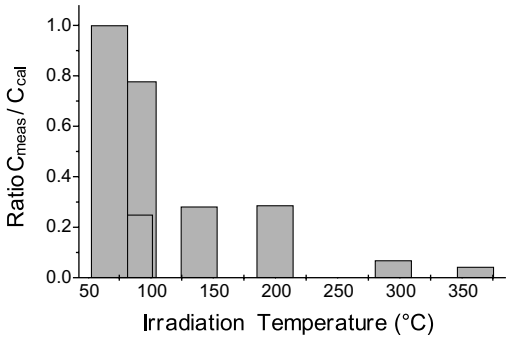

Fig. 12. The temperature dependence of the ratio of the measured hydrogen concentrations to the calculated concentrations.

hydrogen effects should not be an issue, or at least not as important as originally thought, at temperatures above 250 °C in martensitic steels in spallation targets.

References

[1] Y. Dai, G.S. Bauer, J. Nucl. Mater. 296 (2001) 41.
[2] M. Pepin, private communication.
[3] M.R. James, S.A. Maloy, W.F. Sommer, P.D. Ferguson, M.M. Fowler, G.E. Mueller, R.K. Corzine, in: J.G. Williams, D.W. Vehar, F.H. Ruddy, D.M. Gilliam (Eds.), Spectral Unfolding of Mixed Proton/Neutron Fluences in the LANSCE Irradiation Environment, Reactor Dosimetry: Radiation Metrology and Assessment,

ASTM STP 1398, American Society for Testing and Materials, West Conshohocken, PA, 2001, p. 167.
[4] H. Farrar, B.M. Oliver, J. Vac. Sci. Technol. A 4 (1986) 1740.
[5] B.M. Oliver, F.A. Garner, L.R. Greenwood, J. Abrefah, J. Nucl. Mater. 283–287 (2001) 1006.
[6] M. James, Ph. Ferguson, in press.
[7] F.A. Garner, B.M. Oliver, L.R. Greenwood, M.R. James, P.D. Ferguson, S.A. Maloy, W.F. Sommer, J. Nucl. Mater. 296 (2001) 66.
[8] M.H. Barnett, M.S. Wechsler, D.J. Dudziak, R.K. Corzine, L.A. Charlton, L.K. Mansur, in: Proceedings of the 3rd International Topical Meeting on Nuclear Applications of Accelerator Technology (AccApp99), p. 555.
[9] L.R. Greenwood, R.K. Smither, SPECTER: Neutron damage calculations for materials irradiations, ANL/FPP/TM-197, Argonne National Laboratory, January 1985P.
[10] M.B. Chadwick, P.G. Young, S. Chiba, S.C. Frankle, G.M. Hale, H.G. Hughes, A.J. Koning, R.C. Little, R.E. MacFarlane, R.E. Prael, L.S. Waters, Nucl. Sci. Engng. 131 (3) (1999) 293.
[11] X. Jia, Y. Dai, M. Victoria, J. Nucl. Mater. 305 (2002) 1.
[12] Y. Dai, X. Jia, these Proceedings. doi:10.1016/S0022-3115(03)00100-4.
[13] J. Henry, X. Averty, Y. Dai, P. Lamagnère, J.P. Pizzanelli, J.J. Espinas, P. Wident, these Proceedings. doi:10.1016/S0022-3115(03)00119-3.
[14] P. Marmy, B.M. Oliver, private communication.